Research on Atomic Structure and Collision Cross Sections for Spectroscopic Modeling in KAERI Atomic Data Center

Duck-Hee Kwon* and Kil-Byoung Chai†

Nuclear Physics Application Research Division,

Korea Atomic Energy Research Institute, Daejeon 34057, Korea

(Received 31 August 2022)

Abstract

Research activities in KAERI Atomic Data Center on the basic atomic structure and collision cross sections needed for spectroscopy analysis in various atomic and molecular, optical, and plasma physics fields are instructed. The methodologies of our research and the present and future aspects of the applications are explained. In addition, our constructed numerical database for the atomic data and running of a collisional-radiative spectroscopic modeling code on the web are demonstrated.

Keywords: Atomic structure, Collision cross section, Isotope shift, Hyperfine structure, Collisional-radiative modeling, Database

*Electronic address: hkwon@kaeri.re.kr

†Electronic address: kbchai@kaeri.re.kr

I. INTRODUCTION

Atomic structure such as energy levels and radiative transition probabilities of atoms and ions, and collision cross section for atom/ion with charged particles are essential for atomic, optical, and plasma spectroscopies. Our atomic data group in KAERI, nuclear data center has generated the atomic structure and collision data, and modeled spectra, which have been uploaded and run in a database web so called PEARL(Photonic Electronic Atomic Reaction Laboratory, http://pearl.kaeri.re.kr).

In this informative report, our research activities on the atomic data and the spectroscopic modelings are described and the utilization through domestic and international collaborations and networking are promoted. Firstly, features of available atomic codes are listed. Then our methods for the atomic data calculation and the spectroscopic modeling are explained. The PEARL database is presented, together with collaborations in communities of this field. Finally, perspectives of our research group are summarized with the application area of our researches.

II. ATOMIC CODES

Computational atomic codes to calculate energy levels and transition probabilities or collision cross section s can be listed below as classified into non-relativistic and fully relativistic ones.

Non-relativistic codes with relativistic corrections :

- Cowan (R. D. Cowan[1, 2]) and its variations ([3–7])
- MCHF (ATSP2K , C. F. Fischer et al. [8])
- CIV3 (A. Hibbert [9])
- SUPERSTRUCTURE (W. Eissner et al. [10])
- Belfast R-matrix RMATRIX1 (K. A. Berrington et al. [11])
- pseudo-state R-matrix RMPS (K. Bartschat et al. [12])
- B-spline R-matrix (BSR, O. Zatsarinny [13])

- Breit-Pauli AUTOSTRUCTURE (N. R. Badnell [14])

Relativistic codes :

- MCDHF (GRASP2K, GRASP2018, C. Froese Fischer et al. [15])
- MDFGME (J.P. Desclaux and P. Indelicato [16, 17])
- RMBPT (M.S. Safronova et al. [18])
- CCC (I. Bray and D. V. Fursa [19])
- DARC (P. H. Norrington et al. [20, 21]) and pDARC (C. P. Ballance et al. [22])
- ATOM (M. Y. Amusia et al. [23])
- HULLAC (A. Bar-Shalom et al. [24])
- FAC (M. F. Gu [25])
- RATIP and JAC (S. Fritzsche [26, 27])

The legacy Cowan's code uses the non-relativistic HartreeFock method and some of the relativistic effects are treated as perturbations. The radial wavefunctions are computed in a hydrogenic single-configuration approximation, and they are frozen in calculations of configuration interactions while the existant more elaborated multiconfiguration codes such as MCHF, CIV3, MCDHF, MDFGME, and FAC etc. use the radial wavefunctions of each basis configuration varied in the self-consistent field (SCF) calculation. A least-squares fitting (LSF) of atomic energy levels is adopted for adjusting the Slater parameters to fit experimental levels and the adjusted Slater parameters are transferred to the input file of the package computing the angular matrix elements of the Hamiltonian iteratively. This procedure computes more accurate energy levels, transition wavelengths, and radiative rates for the electric-dipole (E1), magnetic-dipole (M1), and electric-quadrupole (E2) transitions. Cowan code is a little primitive but more consistent with experiment.

For heavy elements such as lanthanides and actinides, the ab-initio multiconfiguration methods even fail to reproduce the experimentally known ground states predicting incorrect levels or configurations to be the lowest ones in energy implying that they have computational limitations to treat atomic systems where electron-correlation effects so called configuration

interaction (CI) between closely-lying levels of the same parity and the same J values are large and numerous. This Strong CIs also occur for Rydberg levels as the energies approach the ionization limit. The multiconfiguration methods try to obtain a precise determination of level energies by adding a large number of virtual high-lying configurations. However Cowans codes can attain the LSF of all levels with a standard deviation less than 100 cm^{-1} reproducing all strong line intensities and predicting unknown levels with a similar accuracy [28]. Thus, Cowans codes have been workhorse tools for the past few decades [28] and the recommended values in the NIST spectroscopic database are mostly provided with the modified Cowan code by A. Kramida [7, 29].

The recent ab-initio FAC (flexible atomic code) [25] uses single local central potential for all orbitals which ensures automatic orthogonality between orbital's wavefunctions. This enables more computationally efficient and large CI calculation. While the MC(D)HF and MDFGME take into account for the non-local exchange potential in the SCF calculation. However, the principally inaccurate wavefunction by FAC compared with the full SCF method tends to result in low precision for complex atomic systems like neutral atom.

There are two types of collision codes. One is by the close coupling method (Convergent CC and R-matrix codes), and the other is by perturbative distorted-wave (DW) method (AUTOSTRUCTURE, HULLAC, FAC, RATIP and etc.)

III. ATOMIC DATA CALCULATION

Astrophysical or tokamak plasmas are often in optically thin, low-density, dust-free, in steady or quasi-steady state. The effects of three body recombination, radiation field, density, and charge exchange can be neglected and most ions have the majority of their population in the ground level under these conditions. The charge state distribution (CSD) is determined by the balance of electron-impact ionization (EII) with recombination. This plasma state is typically called collisional ionization equilibrium (CIE). We have calculated EII and dielectronic recombination (DR) for ground and lowest excited levels of various ions which are useful for the determination of CSD in CIE by using the FAC based on the relativistic distorted-wave (DW) approximation. **The calculated atomic data has been uploaded in our PEARL database.** The **theoretical** methods **for the atomic data held by PEARL database** will be described in the following subsections.

A. Electron-impact ionization

EII of A^{q+} ion can occur by direct ionization (DI) and indirect excitation-autoionization (EA), resonant excitation-double autoionization (REDA), and resonant excitation-auto double ionization (READI) as listed below.

- DI : $A^{q+} + e \rightarrow A^{(q+1)+} + e' + e''$
- EA : $A^{q+} + e \rightarrow A^{q+^{**}} + e' \rightarrow A^{(q+1)+} + e' + e''$
- REDA : $A^{q+} + e \rightarrow A^{(q-1)+^{**}} \rightarrow A^{q+^{*}} + e' \rightarrow\rightarrow A^{(q+1)+} + e'' + e'''$
- READI : $A^{q+} + e \rightarrow A^{(q-1)+^{**}} \rightarrow A^{(q+1)+} + e' + e''$

In an independent process-isolated resonance (IP-IR) approximation the total EII cross section for DI, EA, and REDA can be given by [30]

$$\sigma_{\rm tot} = \sum_f \sigma_f^{\rm DI} + \sum_j \sigma_j^{\rm CE} B_j^a + \sum_k \bar{\sigma}_k^{\rm DC} B_k^{da}, \tag{1}$$

where $\sigma_f^{\rm DI}$ represents DI cross section to f level of $A^{(q+1)+}$ ion, $\sigma_j^{\rm CE}$ denotes collisional excitation cross section to multiply excited level j of A^{q+} ion, and $\bar{\sigma_k}^{DC}$ stands for dielectronic capture cross section to multiply excited level k of $A^{(q-1)}+$ ion. The autoionization (AI) branching ratio (BR) B_j^a and the double-AI BR B_k^{da} are expressed as

$$B_j^a = \frac{\sum_s A_{js}^a B_s^r + \sum_t A_{jt}^r B_t^a}{\sum_s A_{js}^a + \sum_t A_{jt}^r}, \; B_k^{da} = \frac{\sum_{j'} A_{kj'}^a B_{j'}^a}{\sum_{j'} A_{kj'}^a + \sum_{t'} A_{jt'}^r}, \tag{2}$$

where A^a and A^r are AI rate and radiative decay (RD) rate, respectively. The DI, CE, and DC cross sections as well as AI and RD rates are calculated from FAC and all of the branching ratios are solved for recursively. The resulting B_j^a and the double-AI BR B_k^{da} are obtained by our post processing program for the FAC outputs.

B. Dielectronic recombination

Electron-impact recombination of ion can occur directly by radiative recombination (RR) expressed as

$$A^{q+} + e \rightarrow A^{(q-1)+} + \hbar\omega, \tag{3}$$

and also indirectly via intermediate autoionizing resonance levels by dielectronic recombination (DR)

$$A^{q+} + e \rightarrow A^{(q-1)+**} \rightarrow A^{(q-1)+} + \hbar\omega. \tag{4}$$

The DR is often dominant in the CIE and we have calculated DR cross sections. Neglecting the interference between RR and DR as well as between DR resonances, the energy averaged DR cross section in the IP-IR and the DW approximations can be expressed in atomic units as [31]

$$\bar{\sigma}_{ij} = \bar{\sigma}_{ij}^{\rm DC} B_j, \tag{5}$$

where $\bar{\sigma}_{ij}^{\rm DC}$ is the dielectronic capture cross section for the recombining level i to the intermediate resonance level j and B_j is the radiative stabilizing branching ratio for the resonance level j. $\bar{\sigma}_{ij}$ can be written as

$$\bar{\sigma}_{ij}^{\rm DC} = \frac{\pi^2}{E_{ij}} \frac{g_j}{2g_i} A_{ji}^a \frac{\Gamma_j/2\pi}{(E-E_{ij})^2 + \Gamma_j^2/4} \simeq \frac{g_j}{2g_i} A_{ji}^a \delta(E - E_{ij}), \tag{6}$$

where g_i and g_j are the statistical weights of the levels i and j, respectively, E_{ij} is the resonance energy, and Γ_j is the total resonance width given by $\Gamma_j = \sum_k A_{jk}^a + \sum_f A_{jf}^r$ for AI rate A_{jk}^a and RD rate A_{jf}^r from the level j to any k and f levels, respectively. B_j is given by

$$B_j = \frac{\sum_t A_{jt}^r + \sum_{t'} A_{jt'}^r B_{t'}}{\sum_k A_{jk}^a + \sum_f A_{jf}^r}. \tag{7}$$

We parallelized the radiative transition probability routine of the original FAC to calculate so many radiative decay channels involved in the radiative stabilizing branching ratio B_j for complex atomic system such as W ions [32].

C. Electron-impact excitation

The cross section for EIE process expressed as $A^{q+} + e \rightarrow A^{q+*} + e'$ is calculated with a DW approximation in FAC which does not include coupling among channels and uses a non-unitarized scattering matrix assuming small reactance matrix. Relativistic DW (RDW) approximation in pure jj-coupling employing those simplifications has been expected to be accurate for highly charged ions or for sufficiently high energies. However, such RDW

approach overestimates the background contribution to the cross section for lowly charged ions or neutral atom and for low energies owing to the omission in channel coupling and the non-unitarity of scattering matrix.

The sophisticated CC methods such as R-matrix and convergent CC are generally more accurate in low and intermediate energy regions than DW methods. However, their dataset is limited due to huge computer resources and cross sections treating resonance as independent process are needed for some plasma modelings. Thereby we performed two types II and III [33] (the inverse and diagonalization forms as mentioned below) of unitarization for the RDW approach by implementing routines for the unitarized scattering matrix into the FAC [25].

The EIE cross section $\sigma_{01}(E)$ for incident electron energy E and initial 0 and final 1 levels can be expressed from the dimensionless collision strength $\Omega_{01}(E)$ by the relation

$$\sigma_{01}(E) = \frac{\pi}{k_0^2 g_0}\Omega_{01}, \tag{8}$$

where k_0 is the relativistic wave number of incident electron given by

$$k_0^2 = E\left[1 + \frac{\alpha^2}{4}E\right] \tag{9}$$

for the fine-structure constant α, and g_0 is the statistical weight of the initial level . The collision strength $\Omega_{01}(E)$ can be given by summation of partial collision strength ${\Omega^{J_T}}_{01}(E)$ for total angular momentum J_T of target and continuum electrons as

$$\Omega_{01} = \sum_{J_T} \Omega_{01}^{J_T}(E). \tag{10}$$

The partial collision strength is defined by

$$\Omega_{01}^{J_T}(E) = \frac{1}{2}\sum_{j_0,j_1}(2J_T+1)|\mathbf{T}^{J_T}(\Gamma_0 J_0 j_0, \Gamma_1 J_1 j_1)|^2, \tag{11}$$

where $\mathbf{T}^{J_T}(\Gamma_0 J_0 j_0, \Gamma_1 J_1 j_1)$ are the transmission matrix elements. $\Gamma_{0,1}$, $J_{0,1}$, and $j_{0,1}$ refer to suppressed quantum numbers, total angular momenta of target state, and total angular momenta of continuum electron, respectively, before and after collision.

The transmission matrix $\mathbf{T}$ can be defined by the Born I, II, and III approximations [33]

$$\mathbf{T}_{\mathrm{I}} = -2i\mathbf{K} \tag{12}$$

$$\mathbf{T}_{\mathrm{II}} = -2i\mathbf{K}/(\mathbf{1} - i\mathbf{K}) \tag{13}$$

$$\mathbf{T}_{\mathrm{III}} = \mathbf{1} - e^{2i\mathbf{K}}, \tag{14}$$

where approximation II needs matrix inversion and approximation III requires matrix diagonalization for reactance matrix $\mathbf{K}$. $e^{2i\mathbf{K}}$ is given by $e^{2i\mathbf{K}} = \mathbf{Y}e^{2i\mathbf{b}}\mathbf{Y}^\dagger$ for a diagonal matrix $e^{2i\mathbf{b}}$ with diagonal elements e^{2ib_j} where b_j is the elements of diagonal matrix $\mathbf{b}$ satisfying $\mathbf{KY} = \mathbf{Yb}$. The reactance matrix elements $\mathbf{K}_{01}^{J_T}$ can be expressed by

$$\mathbf{K}_{01}^{J_T} = 2\sum_{\kappa_0\kappa_1}\langle\psi_0|\sum_{i<j}^{N+1}\frac{1}{r_{ij}}|\psi_1\rangle, \tag{15}$$

where ψ_0 and ψ_1 are the antisymmetrized initial and final states of $N+1$ target and continuum electrons

$$\psi_i = \{\Psi_i(\Gamma_i J_i), \kappa_i; J_T, M_T\}, (i = 0, 1), \tag{16}$$

for the target electron state $\Psi_i(\Gamma_i J_i)$, relativistic quantum number $\kappa_i = (l_i - j_i)(2j_i + 1)$ of continuum electron, and the projection M_T of the total angular momentum J_T.

The FAC uses type I approximation of Eq. 12 assuming small reactance matrix $\mathbf{K}$ elements, but the scattering matrix defined by $\mathbf{S} \equiv \mathbf{1} - \mathbf{T}$ does not satisfy the unitarity condition $\mathbf{S}^\dagger\mathbf{S} = \mathbf{1}$ in general. However, the scattering matrice by type II and III approximations for real and symmetric reactance matrix conserve the unitarity. Routines carrying out matrix inversion and diagonalization for the $\mathbf{K}$ matrix are newly inserted and combined into the original FAC and RDW calculations eliminating a lack of unitarity are enabled by the type II and III approximations [34].

D. Photoionization

The cross section for photoionization (PI) expressed as $A^{q+} + \hbar\omega \rightarrow A^{(q+1)+} + e$ are important for opacity calculation and modeling of astrophysical plasma exposed to hot sources of radiation such as the sun and stellar transition regions. Computationally efficient non-iterative eigenchannel R-matrix (RM) approach connected with multichannel quantum-defect theory by C. H. Green [35] was used. The RM code was modified to calculate the partial cross section by D.-S. Kim [36].

The PI via autoionization channels for Mg-like ions considered are shown in Figure 1(a) and the calculated PI cross section for Ar^{6+} are displayed in Figure 1(b) compared with the opacity database.

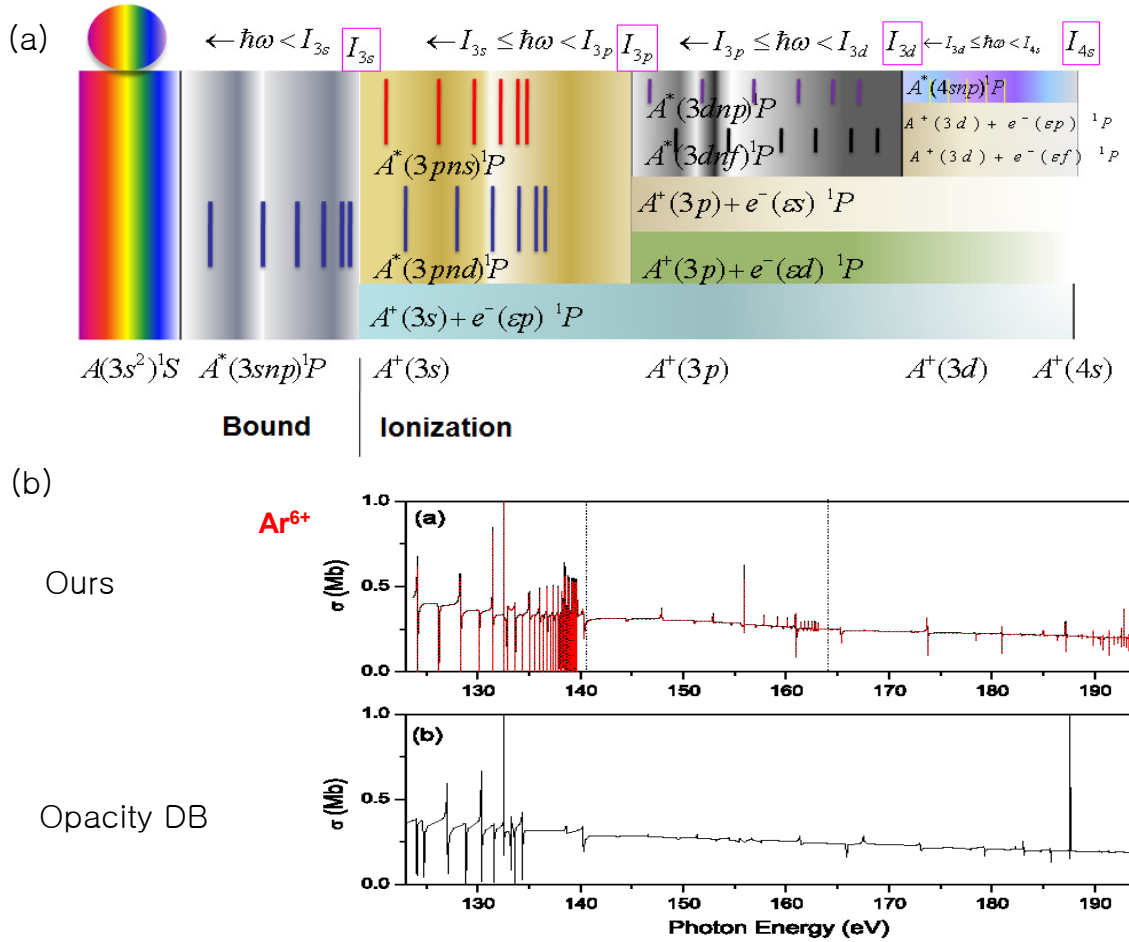

FIG. 1: (Color online) (a) Photoionization of Mg-like ion via autoionization resonances (b) PI cross sections for Mg-like Ar^{6+} by our calculation (black dolid line: length gauge, red dotted line: velocity gauge), and PI cross section in the opacity database

E. Isotope shift and hyperfine structure

Isotope shifts (IS) and hyperfine structure in atomic spectral lines have been of interest to many researchers because they provide information on the nuclear properties of the atoms as well as they have been employed in applications, such as selective photoionization [37].

Is is occurred from nuclear mass shift (MS) and field shift(FS). MS and FS analysis enable to determine the nuclear mass and radius, respectively. Hyperfine structure arises from magnetic dipole interaction and electric quadrapole interaction between nucleus and electrons. From the hyperfine structure nuclear spin and shape can be deduced.

Multi-configuration Dirac-Fock(MCDF) calculations by MDFGME were performed to in-

terpret the FS contributions to isotope shifts of Sm I in visible and near-UV(NUV) transition lines [38]. FS is proportional to the electron charge density at the origin and can be used to test the reliability of *ab initio* calculations on electronic structures. MCDF calculations for the electron charge density at the origin that include the configuration mixing effect agreed well with the electronic factor ratios derived from experimental data.

The IS and hyperfine structure studies by theoretical calculation has been extended to analyze the collinear laser spectroscopy (CLS) in the RAON (Rare isotope Accelerator complex for ON-line experiment) heavy particle accelerator.

IV. SPECTROSCOPIC MODELING

We have carried out spectroscopic modeling for high and low temperature plasmas. For high temperature plasmas in the CIE, the optical line spectra can be calculated with a coronal approximation including only EIE from ground level and radiative decays. However, for low temperature plasmas collisional-radiative modeling (CRM) including possible other collisional and radiative processes besides the EIE from ground level and radiative decays in detail is needed for the population kinetics and the intensities of the line spectra. Our methods for the coronal approximation and the CRM are instructed below.

A. Photon emission coefficient for W ions

With the coronal approximation, the photon emissivity ϵ_{ij} for optical line transition from i to j is defined by

$$\epsilon_{ij} = n_Z(r,t) n_e(r,t) PEC_{ij}(T_e, n_e), \tag{17}$$

where n_Z and n_e denote charge Z ion density and electron density, respectively, and PEC_{ij} denotes photon emissivity coefficient (PEC) from level i to level j. The PEC in the coronal approximation is given by

$$PEC_{ij}(T_e) = \alpha_{0i}^{\rm ex} \frac{A_{ij}}{\sum_{k<i} A_{ik}}, \tag{18}$$

where $\alpha_{0i}^{\rm ex}$ denotes the EIE rate from the ground level 0 to the level i, A_{ij} is the RD rate from the level i to j, and A_{ik} is the RD rate from the level i to any level k lower than the level i.

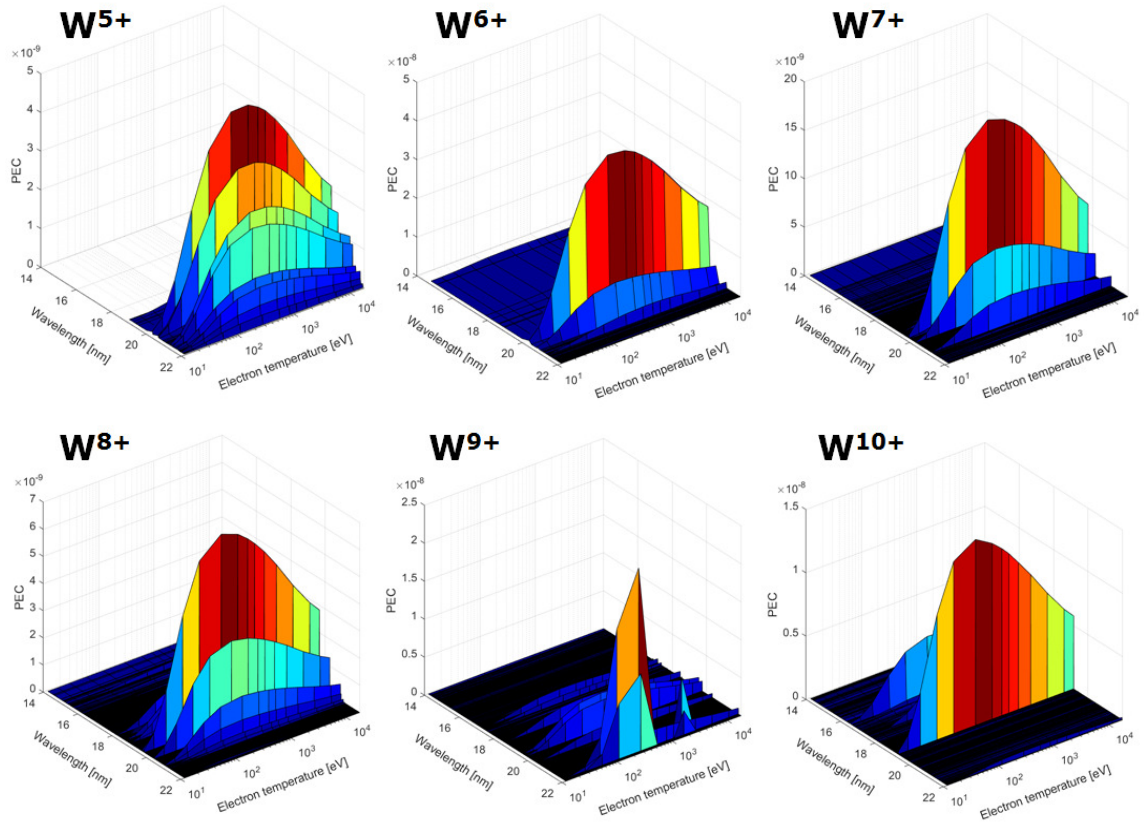

FIG. 2: (Color online) PEC calculated with the coronal approximation for $W^{5+}-W^{10+}$ ions.

We used our own modified FAC with parallelized radiative transition probability routine to calculate so many radiative transition rates for tungsten (Z=74) ions. Figure 2 shows the calculated PEC for selected W ions. Our calculated PEC for $W^{5+}-W^{48+}$ ions was used for spectroscopic analysis of impurity transport in KSTAR tokamak by the KAIST Gas Discharge Physics Laboratory (http://gdpl.kaist.ac.kr)

B. CRM for low temperature Ar and He plasmas

In the case of weakly ionizing plasma of $n_0\alpha_{\rm I} \gg n_+\alpha_{\rm R}$ for the neutral n_0 and the ion n_+ densities and the ionization $\alpha_{\rm I}$ and the recombination $\alpha_{\rm R}$ rates, The excited level i population

N_i of the neutral atom can be determined by the steady-state balance equation

$$\sum_{j\neq i} n_e \alpha_{ji}^{\mathrm{ex}} N_j + \sum_{j>i} \eta_{ji} A_{ji} N_j = \sum_{j\neq i} n_e \alpha_{ij}^{\mathrm{ex}} N_i + \sum_{j<i} \eta_{ij} A_{ij} N_i + n_e \alpha_i^{\mathrm{I}} N_i + \sum_j \alpha_{ij}^{\mathrm{I}} N_i N_j + \nu_i^{\mathrm{d}} N_i, \quad (19)$$

where the left-hand side and the right-hand side correspond to the populating and the depopulating terms of the level i, respectively, for electron density n_e. The parameters for the atomic process in the balance equation are listed as

- Radiative decay: λ_{ij} (wavelength) and A_{ij} (transition probability), η (radiation trapping, escape factor)
- Electron impact excitation/de-excitation rate $\alpha_{ij}^{\mathrm{ex}}$
- Electron impact ionization rate α_i^{I}
- Heavy particle collisional ionization α_{ij}^{I}
- Diffusion ν_i^d

The sources of literatures and databases for the atomic process cross sections and rates are noted in the papers for Ar [39] and He [40]. For rate coefficient calculation from the cross section a non-Maxwellian electron energy distribution function (EEDF) [41] which is often observed in non-equilibrium, low temperature plasmas as well as Maxwellian EEDF, is considered. The escape factor for radiation trapping is taken into account for a finite size cylinder geometry as well as plane parallel and infinite cylinder geometries.

The ground level population $N_0 \simeq n_0$ is determined with the ideal gas law $p = n_0 k_{\mathrm{B}} T_g$ for gas pressure p, the Boltzman constant k_{B} and gas temperature T_g. The balance equation Eq. 19 including the nonlinear terms $\eta_{ji} A_{ji} N_j$ and $\alpha_{ij}^{\mathrm{I}} N_j N_i$ is solved by the multidimensional secant Broydens method [42] setting the initial N_i as the solution of the linear part of Eq. 19.

The relative line intensity I_{ik}^{CRM} to a reference transition is given by

$$I_{ik}^{\mathrm{CRM}} = \frac{\lambda_{ref} N_i \eta_{ik} A_{ik}}{\lambda_{ik} N_{ref} \eta_{ref} A_{ref}}, \quad (20)$$

and the determination of the electron temperature T_e and and density n_e for a plasma by optical emission spectroscopy (OES) and CRM is carried out by finding the variables that minimize the difference

$$\Delta(n_e, T_e, R_{eff}, L_{eff}) = \Sigma \left(\frac{I_{ik}^{\mathrm{CRM}} - I_{ik}^{\mathrm{OES}}}{I_{ik}^{\mathrm{OES}}} \right)^2, \quad (21)$$

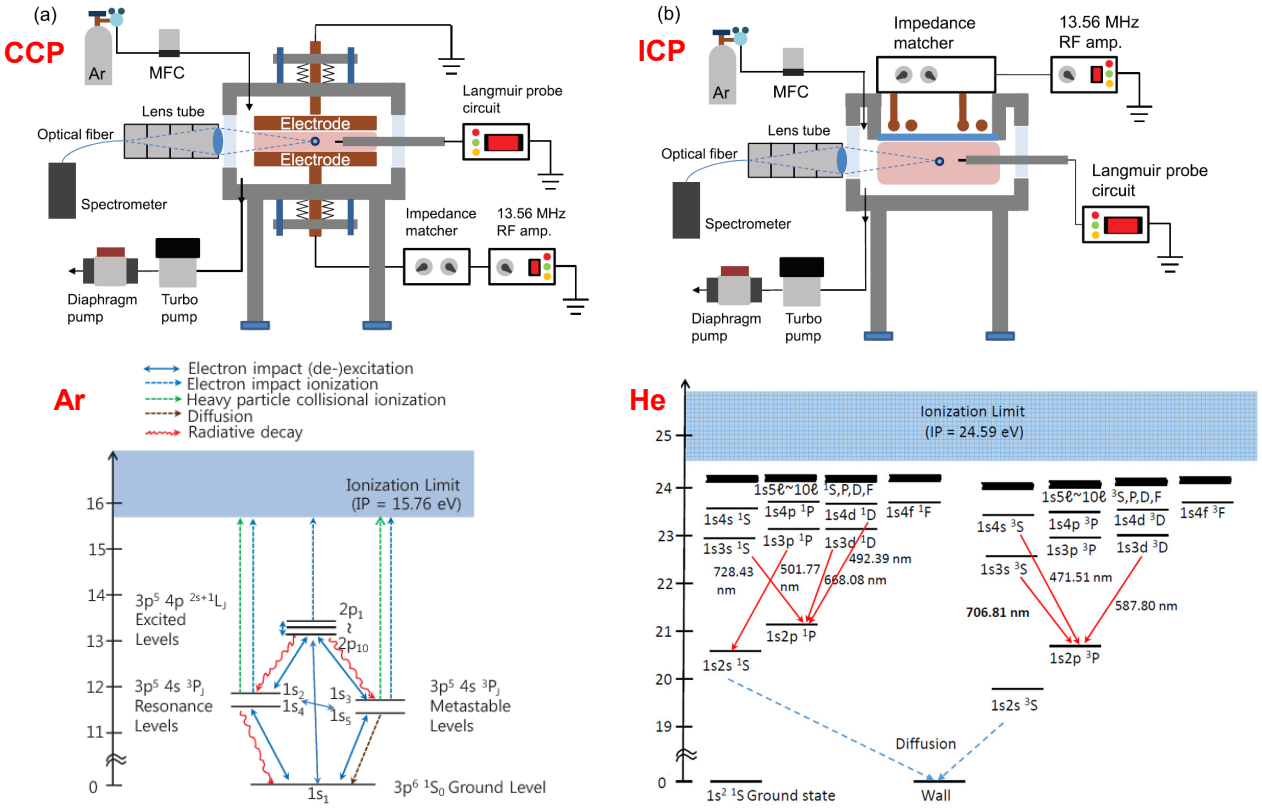

FIG. 3: (Color online) Sketch of our plasma source, OES and LP systems for (a) CCP and (b) ICP. Energy levels included in the CRM for Ar and He are displayed in the bottom figures.

where I_{ik}^{OES} is the measured spectral line intensity for the $i \rightarrow k$ transition relative to the reference transition.

We built our own capacitively-coupled plasma (CCP) device shown in Figure 3(a) which can be switched to ICP device shown in Figure 3(b) easily, in order to test the reliability of the OES diagnostics combined with the CRM by comparing with a Langmuir probe (LP) measurement. The energy level diagrams for Ar I and He I taken into account for our CRM are also shown in Figure 3. The resulting spectra intensities by the OES and the CRM, and diagnostics for electron temperature in the range of 1-5 eV and density in the range of $10^9 - 10^{12}(1/cm^3)$ are shown **in Figure 4 for He and in Figures (5) and (6) of the paper [39] for Ar.**

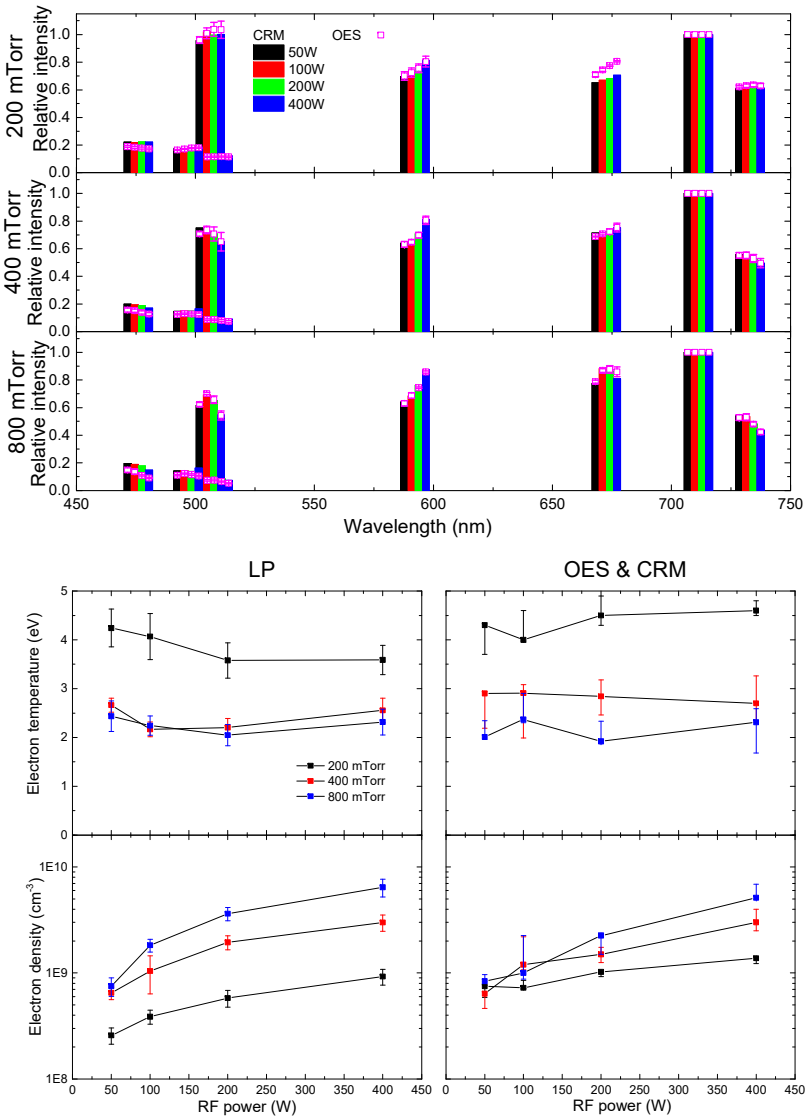

FIG. 4: (Color online) The spectra intensities (upper panel), and the electron temperature and density diagnostics (lower panel) for He-ICP depending on the gas pressure and the RF power.

V. PEARL DATABASE AND NETWORKS FOR ATOMIC DATA EXCHANGE

We have uploaded our generated atomic data together with other available data for comparison on the web so called PEARL (http://pearl.kaeri.re.kr) in the manner of graphically and numerically easy access. The type of our database is demonstrated in Figure 5.

Present contents of atom and ion species uploaded are listed as

- EII : P-like P, S^{+}, Cl^{2+}, Ar^{3+}, $\cdots$, Fe^{11+}, Co^{12+}, Ni^{13+}, Cu^{14+}, Zn^{15+}, and W^{+}, W^{17+}

- DR : Na-like Ca^{9+}, Ti^{11+}, $\cdots$, Fe^{11+}, Co^{12+}, Ni^{13+}, Cu^{14+}, Zn^{15+}, and $W^{44+}-W^{46+}$
- EIE : He
- PI : Be-like Be, B^{+}, C^{2+}, N^{3+}, O^{4+}, F^{5+}, Ne^{6+}, and Mg-like Mg, Al^{+}, Si^{2+}, S^{4+}, Cl^{5+}, Ar^{6+}

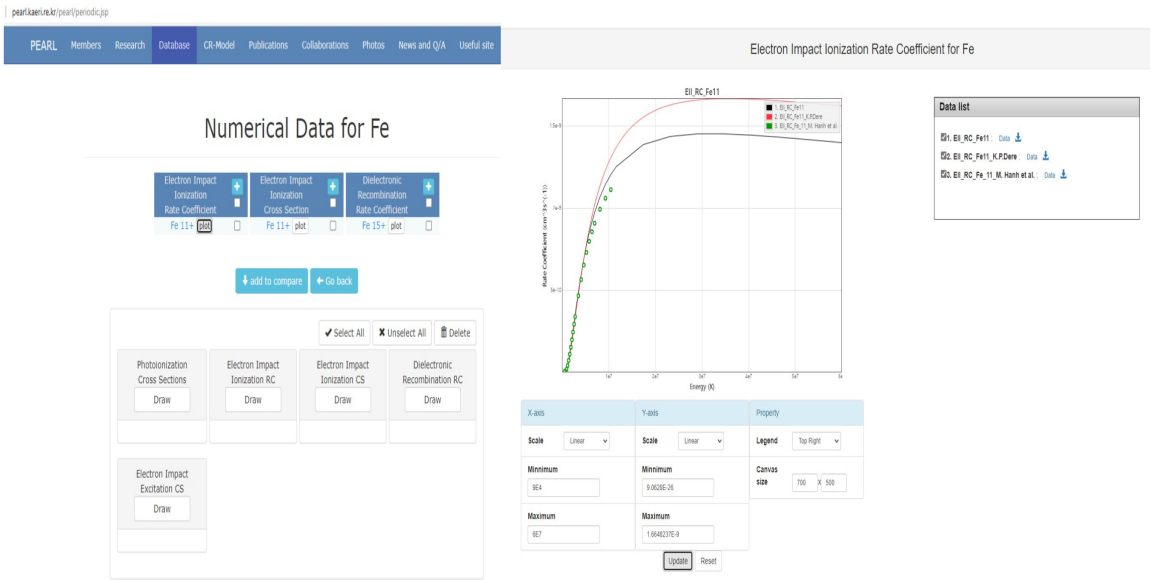

FIG. 5: (Color online) Selected display of our PEARL database for Fe ion.

The EII, DR, and PI data provide for the ground or the lowest metastable levels while the EIE data include excitations between all levels considered in our CRM. DR for $W^{5+}-W^{10+}$ and EIE for Ar and Ar^{+} by the unitarized DW calculation will be uploaded in the near future.

The huge PEC data for W ions including many EIE and RD levels by coronal approximation will be added on the web. We also implemented a CRM program on the PEARL web which enables to get line intensity for He as a function of electron density and temperature. However, the CRM was based on the the model of Fujimoto and Goto [43, 44]. Their model solved the linear steady-state population balance equation and does not consider heavy particle collisions. Moreover, the radiation trapping (reabsorption) effect was taken into account for the photoexcitation only from the ground level within the frame work

of a linear problem, which is not suitable for general plasma conditions. On the other hand, our newly developed CRM for low temperature plasma solves the intrinsic nonlinear balance equation including the heavy particle collisions between the excited levels and the radiation trapping for all the possible radiative transitions self-consistently. The new CRM will be made to run in the web in the near future.

The data of isotope shifts and hyperfine structure useful for discovering properties of nuclides will be planed for uploading in the web.

There are international networking organizations for atomic database exchange and the IAEA AMD unit (International Atomic Energy Agency, Atomic and Molecular Data, Vienna, Austria. https://www-amdia.iaea.org) and VAMDC (Virtual Atomic and Molecular Data Centre, https://vamdc.org) are the representative ones. The IAEA AMD unit aims at establishing and maintaining internationally recommended AMD such as atomic and molecular collision and radiative processes, atomic and molecular structure characteristics, particle-solid surface interaction processes and physico-chemical and thermo-mechanical material properties specially for use in fusion energy research and also other plasma science and technology applications. The VAMDC consortium shares a common technical and political framework for the distribution of AMD and provides access to a broad range of AMD compiled within a set of AM databases accessible through the provision of a single portal. Our group is the member of the organizations and have participated in their facilitating collaborative international research for the production and evaluation of AMD.

VI. SUMMARY AND OUTLOOK

We have carried out state-of-the-art calculations for atomic data such as electron-impact excitation/ionization, dielectronic recombination, and photo ionization for spectroscopic modeling in astrophysical and laboratory plasmas.

The FAC code based on a relativistic distorted approximation has been used, post-processed, and modified as parallel for radiative transition routine. In addition, the unitarity correction for the distorted wave approximation employed in the original FAC routine of the electron impact excitation calculation was implemented. For photoionization cross section the non-iterative eigenchannel R-matrix code improved for enabling the partial cross section was used for Mg-like atom and ions. Multiconfiguration Dirack-Fock calculations for the

isotope shifts of Sm I were performed with the MDFGME code. And the theoretical isotope and hyperfine structure calculations for stable or rare isotopes atoms or ions interested in the collinear laser spectroscopy on the RAON facility will be performed in the near future.

As well, we have developed spectroscopic modeling tools by coronal approximation and by considering detailed collisional-radiative processes. The photon emissivity coefficients for tungsten ions were calculated with the atomic data by the FAC in the coronal approximation and they were provided for an impurity transport modeling of KSTAR tokamak. A collisional-radiative modeling (CRM) program to solve nonlinear balance equation beyond the linear problem framework for low temperature plasma was applied to the OES diagnostic of electron temperature and density for Ar and He in our CCP and ICP. And it was tested with LP measurement. This CRM has been extended for H/D plasma including H_2/D_2 molecules, and H^+/D^+, H_2^+/D_2^+, H_3^+/D_3^+ ions in our unique PBIF (Plasma Beam Irradiation Facility) based on the AF-MPD (applied-field magnetoplasmadynamic) thruster concept [45].

Our atomic data and spectroscopic modeling has been uploaded and implemented in the PEARL web and which has been extensively utilized by collaborating with the international IAEA AMD unit and VAMDC consortium.

Acknowledgments

The authors would like to acknowledge support by the KAERI Institutional Program (Projoect No. 524410-22).

---

[1] R. D. Cowan, *The Theory of Atomic Structure and Spectra* (University of California Press, Berkeley and LA, 1981).

[2] C. McGuinness, *R. D. Cowans Atomic Structure Code* (Trinity College, University of Dublin: Dublin, Ireland, 2007). Available online: https://www.tcd.ie/Physics/people/Cormac.McGuinness/Cowan/).

[3] P. Quinet, P. Palmeri and E. Bimont, J. Quant. Spectrosc. Radiat. Transf. **62** 625 (1999).

[4] R. L. Kurucz, *Atoms* (Harvard University: Cambridge, MA, USA, 2017); Available online : http://kurucz.harvard.edu/atoms.html.

[5] J. Ruczkowski, M. Elantkowska, J. Dembczynski, J. Quant. Spectrosc. Radiat. Transf. **145** 20 (2014).

[6] J. Abdallah, Jr., R.E.H. Clark and R. D. Cowan, *Theoretical Atomic Physics Code Development I. CATS : Cowan Atomic Structure Code* (Report LA-11436-M; Los Alamos National Lab: Los Alamos, NM, USA, 1988). Volume I, p. 31; Available online : https://fas.org/sgp/othergov/doe/lanl/docs3/00323386.pdf

[7] A. Kramida, *A Suite of Atomic Structure Codes Originally Developed by RD Cowan Adapted for Windows-Based Personal Computers* (National Institute of Standards and Technology: Gaithersburg, MD, 2018).

[8] C. F. Fischer, G. Tachiev, G. Gaigalas and M. R. Godefroid, Comput. Phys. Commun. **176** 559 (2007).

[9] A. Hibbert, Comput. Phys. Commun. **9** 141 (1975).

[10] W. Eissner, M. Jones, H. Nussbaumer, Comput. Phys. Commun. **8** 270 (1974).

[11] K. A. Berrington, W. B. Eissner and P. H. Norrington, Comput. Phys. Commun. **92** 290 (1995).

[12] K. Bartschat, E. T. Hudson, M. P. Scott, P. G. Burke and V. M. Burke, J. Phys. B: At. Mol. Opt. Phys. **29** 115 (1996).

[13] O. Zatsarinny, Comput. Phys. Commun. **174** 273 (2006).

[14] N. R. Badnell, Comput. Phys. Commun. **182** 1528 (2011); Available online: http://amdpp.phys.strath.ac.uk/autos

[15] C. F. Fischer, G. Gaigalas, P. Jnsson, J. Bieron, Comput. Phys. Commun. **237** 184 (2019).

[16] J. P. Desclaux, Comput. Phys. Commun. **9** 31 (1975).

[17] P. Indelicato, J. P. Santos, S. Boucard and J. P. Desclaux, Eur. Phys. J. D **45** 155 (2007).

[18] U. I. Safronova, M. S. Safronova and M. G. Kozlov, Phys. Rev. A **76** 022501 (2007).

[19] I. Bray and D. V. Fursa, Phys. Rev. Lett. **76** 2674 (1996).

[20] P. H. Norrington and I. P. Grant, J. Phys. B: At. Mol. Opt. Phys. **20** 4869 (1987)

[21] S. Ait-Tahar, I. P. Grant and P. H. Norrington, Phy. Rev. A **54** 3984 (1996).

[22] C. P. Ballance and D. C. Griffinc, J. Phys. B: At. Mol. Opt. Phys. **39** 3617 (2006); Available online : http://connorb.freeshell.org

[23] M. Y. Amusia and L. V. Chernysheva, *Computation of atomic processes: A handbook for ATOM programs* (IOP publishing, Bristol, UK, 1997).

[24] A. Bar-Shalom, M. Klapish and J. Oreg, J. Quant. Spectrosc. Radiat. Transf. **71** 169 (2001).

[25] M.F. Gu, Can. J. Phys. **86** 675 2008.

[26] S. Fritzsche, Comput. Phys. Commun. **183** 1525 (2012).

[27] S. Fritzsche, Comput. Phys. Commun. **240** 1 (2019).

[28] A. Kramida, Atoms **7**, 64 (2019).

[29] A. Kramida, Fusion Sci. Technol. **63** 313 (2013).

[30] D.-H. Kwon and D. W. Savin, The Astrophysical J. **784** 13 (2014).

[31] D.-H. Kwon and D. W. Savin, Phys. Rev. A **83** 012701 (2011).

[32] D.-H. Kwon, J. Quant. Spectrosc. Radiat. Transf. **208** 64 (2018).

[33] M. J. Seaton, Proc. Phys. Soc. **77** 174 (1961).

[34] D.-H. Kwon and Y.-S. Cho, Atom. Data Nucl. Data **137** 101385 (2021).

[35] C. H. Greene and C. Jungen, Adv. At Mol. Phys. **21** 51 (1985).

[36] D.-S. Kim and D.-H. Kwon, J. Phys. B: At. Mol. Opt. Phys. **48** 105004 (2015)

[37] A. S. Choe, Y.-J. Rhee, J. Lee, M. A. Kuzmina and V. A. Mishin, J. Phys. B: At. Mol. Opt. Phys. **28** 3805 (1995)

[38] D.-H. Kwon, H. Park and Y.-J. Rhee, J. Opt. Soc. Am. B **22** 1123 (2005).

[39] K.-B. Chai and D.-H. Kwon, J. Quant. Spectrosc. Radiat. Transf. **227** 136 (2019).

[40] K.-B. Chai and D.-H. Kwon, Spectrochimica Acta Part B: Atomic Spectrocopy **183** 106269 (2021).

[41] V.A. Godyak, IEEE Trans. Plasma Sci. **34** 755 (2006).

[42] W. H. Press, S. A. Teukolsky, W. T. Vetterling and B.P. Flannery, *Numerical recipes in C: The art of scientific computing* (2nd Ed. Cambridge University Press, 1992).

[43] T. Fujimoto, J. Quant. Spectrosc. Radiat. Transfer **21** 439 (1979).

[44] M. Goto, J. Quant. Spectrosc. Radiat. Transfer **76** 331 (2003).

[45] K.-B. Chai, D.-H. Kwon and M. Lee, Plasma Phys. Control. Fusion **63** 125020 (2021).